

Cite this article as: Xing Hairui, Shi Qianshuan, Hu Boliang, et al. Solid-Solution Heat Treatments Effect on Microstructure and Mechanical Properties of Low-Oxygen TZM Alloy[J]. Rare Metal Materials and Engineering, 2025, 54(03): 593-603. DOI: <https://doi.org/10.12442/j.issn.1002-185X.20240560>.

ARTICLE

Solid-Solution Heat Treatments Effect on Microstructure and Mechanical Properties of Low-Oxygen TZM Alloy

Xing Hairui¹, Shi Qianshuan^{1,4}, Hu Boliang¹, Li Shilei^{1,3}, Li Yanchao³, Wang Hua², Wang Qiang⁴, Xu Liuji⁵, Feng Rui⁴, Zhang Wen³, Hu Ping¹, Wang Kuaishe¹

¹National and Local Joint Engineering Research Center for Functional Materials Processing, College of Metallurgical Engineering, Xi'an University of Architecture and Technology, Xi'an 710055, China; ²School of Environmental and Municipal Engineering, Xi'an University of Architecture and Technology, Xi'an 710055, China; ³Institute of Refractory Metals Materials, Northwest Institute for Nonferrous Metal Research, Xi'an 710016, China; ⁴Western Xinxing Rare and Precious Metals Co., Ltd, Shangluo 726100, China; ⁵National Joint Engineering Research Center for Wear Control and Forming of Metal Materials, Henan University of Science and Technology, Luoyang 471003, China

Abstract: Low-oxygen TZM alloy (oxygen content of 0.03vol%) was subjected to solid-solution heat treatment at various temperatures followed by quenching. Results show that the tensile strength of the alloy gradually decreases with the increase in solid-solution temperature, and the elongation first increases and then decreases. The amount of nanoscale Ti-rich phases precipitated in low-oxygen TZM alloys gradually increases with the increase in solid-solution temperature. Special strip-shaped Ti-rich areas appear in the samples solidified at 1200 and 1300 °C. The nanoscale Ti-rich phases ensure the uniform distribution of dislocations throughout TZM alloy, while significantly improving the plasticity of low-oxygen TZM alloy samples.

Key words: TZM alloy; solid-solution; quenching; microstructure evolution; mechanical properties

1 Introduction

Molybdenum (Mo) is a silvery-white refractory metal with a melting point of 2620 °C. Due to its good high-temperature strength, creep resistance, thermal conductivity, corrosion resistance, and low coefficient of thermal expansion, it is widely used in aerospace, electronics, new energy sources, semiconductor lighting, medical devices, and other important industrial fields^[1-4]. Nevertheless, Mo typically exhibits poor ductility and toughness at room temperature, making it prone to brittle fracture, which severely restricts the feasibility of deep processing and the range of applications of Mo^[5-8]. The studies have shown that alloying is an effective method to improve the room temperature brittleness of pure Mo materials, usually through solid-solution strengthening, dispersion strengthening, and composite strengthening^[6-9]. For

this purpose, a series of Mo alloys have been developed, such as Mo-Ti, Mo-Zr, Mo-La, Mo-Y, Mo-Ce, TZM, TZC, and MHC^[10-15]. Among them, TZM alloy is one of the most widely used Mo alloys.

In fact, TZM alloys are extremely prone to oxidation, and the presence of oxygen in TZM alloy increases the possibility of carbides transforming into oxides, even hinders the dispersion of alloy elements and leads to the occurrence of cracks, which results in a sharp decrease in tensile strength and elongation of the material, thereby affecting material properties^[16-18]. Generally, the oxygen content of TZM alloys can be reduced by increasing the carbon content, but the addition of too much carbon will lead to excessive carbon content in Mo alloys, and brittle phases such as large-size MoC may appear in the alloys, which will lead to deterioration of their machinability, and the decrease in

Received date: August 28, 2024

Foundation item: Outstanding Doctorate Dissertation Cultivation Fund of Xi'an University of Architecture and Technology (160842012); National Natural Science Foundation of China (52404409, 52374401, 52104382); China Postdoctoral Science Foundation (2024MD753961); Scientific and Technological Innovation Team Project of Shaanxi Innovation Capability Support Plan (2022TD-30); Key R&D Plan of Shaanxi Province (2023JBGS-14, 2024QCYKXJ-116); Xi'an Science and Technology Plan Project (24ZDCYJSGG0043, 2023JH-GXRC-0020)

Corresponding author: Hu Ping, Ph. D., Professor, National and Local Joint Engineering Research Center for Functional Materials Processing, College of Metallurgical Engineering, Xi'an University of Architecture and Technology, Xi'an 710055, P. R. China, E-mail: huping1985@126.com

Copyright © 2025, Northwest Institute for Nonferrous Metal Research. Published by Science Press. All rights reserved.

mechanical properties and unqualified chemical composition^[19-20]. In the process of regulating the oxygen content of TZM alloy, when the oxygen content of TZM alloy is reduced, the secondary phase in the alloy will decrease significantly. The corresponding strengthening mechanism changes from the secondary phase dispersion strengthening to the solid-solution strengthening, and the fracture mechanism will also change accordingly, from the intergranular fracture of the high-oxygen content alloy to the particle mixed fracture of the low-oxygen content alloy^[21-23].

Solid-solution treatment, as an important heat treatment method, involves heating the alloy to a suitable temperature above the solubility curve and below the solidus line for a certain period to dissolve the secondary phase into a solid-solution. The alloy is then rapidly cooled in water or other media to suppress the reprecipitation of the secondary phase, resulting in supersaturated solid-solutions at room temperature or solid-solution phases that typically only exist at elevated temperatures. Studies have shown that solid-solution quenching treatment of alloys in a certain temperature range can effectively improve the strength and toughness of alloys and play a positive role in material properties^[23-25]. The rapid cooling treatment after solid-solution can make the strong toughness of the alloy and improve the strength at the same time^[26].

In this study, low-oxygen TZM alloy was prepared by powder metallurgy method, and element C was introduced through solid-liquid doping. It was subjected to heat treatment of solid-solution quenching at different temperatures after rolling. The properties of the material were tested using uniaxial tension and three-point bending methods, and the changes in microstructure were analyzed by scanning electron microscope (SEM), electron backscatter diffraction (EBSD), and transmission electron microscope (TEM). The influence of solution temperature on the properties and microstructure of low-oxygen TZM alloy was analyzed. The importance of improving the mechanical properties of TZM alloy with appropriate solution temperature was clarified, which has profound reference significance for practical applications. This study has important theoretical and practical significance for guiding the design optimization of alloy materials, selecting heat treatment processes, and predicting performance.

2 Experiment

The raw materials required for the preparation of low-oxygen TZM alloys designed in this experiment are as

follows: high-purity Mo powder, model FMo-1 (purity \geq 99.80%), oxygen content of 0.17vol%, TiH₂ powder, ZrH₂ powder with particle size about 50 μ m, grayish-black in appearance, grades THP20-1 (TiH₂) and FZH (ZrH₂). The chemical composition of raw materials is listed in Table 1. The experiments were conducted using powder metallurgy, where Ti and Zr were added to Mo powder in the form of TiH₂ and ZrH₂, and C was added in the form of fructose solution by solid-liquid mixing.

After the preparation of raw materials, it was placed in a three-dimensional mixer for 3 h, mixed with the alloy powder for hydrogen reduction, followed by LDJ2150/3000-250YS cold isostatic press to prepare the billet. Then, it was sintered in a high temperature hydrogen preservation furnace at 2000 °C. The thickness of the Mo alloy sintered billet was 15 mm. Sintered billets were opened at 1350 °C, and low-oxygen TZM alloy billets with a thickness of 1.5 mm were prepared by rolling. The total deformation of rolling was 90%, and the rolling process is shown in Table 2, where *H* and *h* represent the thickness before and after rolling, respectively. Before rolling, sintered billets were heated at 1300 °C for 40 min. After 3 passes, the billets needed to heat at 1300 °C for 30 min. After 6 passes, the billets were annealed at 850 °C for 120 min, alkaline washed, trimmed and then heated at 400 °C for 10 min. Finally, low-oxygen TZM alloy sheet with a thickness of 1.50 mm was obtained.

The solid-solution quenching was carried out in a tube atmosphere furnace. The TZM alloys are heated to 1000, 1100, 1200 and 1300 °C at a heating rate of 10 °C/min in an argon environment, and then subjected to solid-solution treatment with a holding time of 12 h. It is quickly removed and placed in pre-prepared ice water for quenching treatment.

The oxygen content of the TZM alloy was determined by an oxygen and nitrogen analyzer. Uniaxial tensile and three-point bending samples were prepared according to the standard. And the experiments were carried out on the electronic universal testing machine. The tensile sample was taken at the length of 25 mm, the width of 6 mm, and tensile speed of 0.5 mm/min. Three-point bending sample had a length of 40 mm, a width of 6 mm, a span of 30 mm, and a loading rate of 0.5 mm/min. The samples under various states of the test were observed morphologically by SEM with a field emission gun equipped with an Oxford instrument EBSD. The obtained results were analyzed using Channel 5 software. The SEM 500 (Germany) and field emission TEM (Talos F200X) with an energy dispersive spectrometer (EDS) were used to analyze the distribution and chemical composition of the secondary

Table 1 Chemical composition of raw material alloy powder (wt%)

Mo powder (FMo-1)	Al	Ca	Fe	Ni	Si	C	O	N	Mo
	0.0015	0.0015	0.005	0.003	0.002	0.005	0.017	0.015	99.90
TiH ₂ powder (THP20-1)	H	Cl	N	Si	C	Fe	Mg	Mn	Ti
	3.84	0.05	0.05	0.02	0.02	0.06	0.01	0.01	91.92
ZrH ₂ powder (FZH)	(Zr+Hf)+H		Zr+Hf	H	Fe	Ca	Mg	Cl	Si
	\geq 98		\geq 96	\leq 1.87	\leq 0.16	\leq 0.03	\leq 0.08	\leq 0.04	\leq 0.07

Table 2 Rolling process of low-oxygen TZM alloy billets

Pass	Rolling size/mm		Pass reduction/%
	<i>H</i>	<i>h</i>	
1–2	15.00	10.50	30
3	10.50	7.56	25
4–6	7.56	3.00	60
7– <i>N</i>	3.00	1.50	50 (<10%/pass)

phase. The distribution of elements, changes in grain size, and grain orientation in TZM alloys with different oxygen contents were characterized by EBSD.

3 Results and Discussion

3.1 Tensile properties and fracture morphology

The microstructure and morphology of low-oxygen TZM sintered billet are shown in Fig.1. And the stress-strain curves of low-oxygen TZM alloy plate after solid-solution quenching at different temperatures are shown in Fig.2. It can be seen that with the increase in solution temperature, the tensile strength of low-oxygen TZM alloy gradually decreases, and the elongation first increases and then decreases (Fig.2).

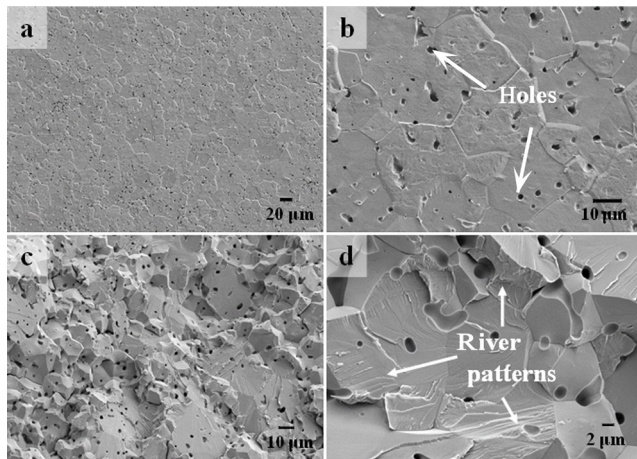


Fig.1 Microstructures of sintered low-oxygen TZM alloybillet: (a–b) surface morphologies; (c–d) fracture morphologies

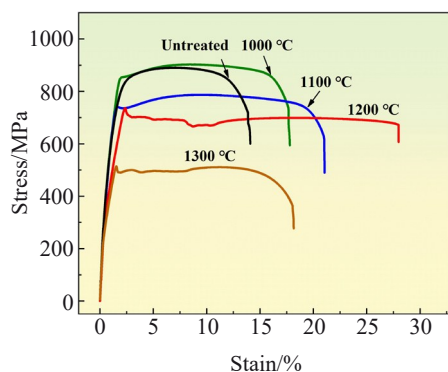


Fig.2 Stress-strain curves of low-oxygen TZM alloy sheets after solid-solution quenching at different temperatures

The alloy treated at 1000 °C has the highest tensile strength (902 MPa), which is basically consistent with the strength of the sample without solid-solution treatment, but the elongation (17.8%) is significantly higher than that of the non-solid solution sample, indicating that the solid-solution quenching has a significant improvement effect on the plasticity of low-oxygen TZM alloy. The highest elongation of the alloy treated at 1200 °C is about 28.1%, but as the solution temperature increases, the alloy gradually undergoes recrystallization and the strength relatively decreases to 736.1 MPa. Compared with other samples, the comprehensive performance of the sample treated at 1200 °C is the best. The strength and elongation of the solid-solution sample at 1300 °C decrease significantly compared to the sample treated at 1200 °C, indicating that the quenching heat treatment of the solid-solution significantly improves the plasticity of low-oxygen TZM alloy. Compared with the sample treated at 1200 °C, the strength and elongation of the sample treated at 1300 °C significantly decrease, indicating that excessive temperature will make the comprehensive performance of the low-oxygen TZM alloy decrease.

It is noteworthy that the samples treated at 1200 and 1300 °C show a significant yield phenomenon during room temperature stretching, corresponding to the repeated up and down zones in the tensile curves. The prerequisite for the occurrence of yield phenomenon is that the metallic material contains a certain number of solute atoms to hinder the movement of dislocations via pinning effect. This is exemplified by the yield behavior of low-oxygen TZM alloy after solid-solution quenching, which confirms that an appropriate number of solute atoms are solidly dissolved in the Mo matrix.

The tensile fracture morphologies of low-oxygen TZM alloy plates after solid-solution quenching at different temperatures are shown in Fig.3. Macroscopic analysis of the tensile fracture after treatment at different temperatures shows that the fracture surface of low-oxygen TZM alloy after solution quenching is dull, without obvious visible plastic deformation such as necking. The fracture surface of the sample after solution quenching at 1000, 1100, and 1300 °C presents a fibrous layered structure. The fracture after solution quenching at 1200 °C is relatively flat and glossy, without longitudinal cracks and obvious layered structure. Observing under a high-magnification microscope, the sample is mainly composed of torn fiber layers after solid-solution treatment at 1000 °C, with a few areas showing single small and tough nest-like structures. With the increase in solid-solution temperature, the sample treated at 1100 °C begins to exhibit deconvolution fracture mode. It indicates that a few areas of the alloy have begun to undergo recrystallization, which corresponds to an increase in the plasticity of the sample. The fracture morphology of the sample treated at 1200 °C is mainly deconvolution fracture, in which a large number of river-like patterns can be observed, and many deconvolution steps can also be seen. A large number of river-like patterns can be observed on the fracture surface, and at the same time,

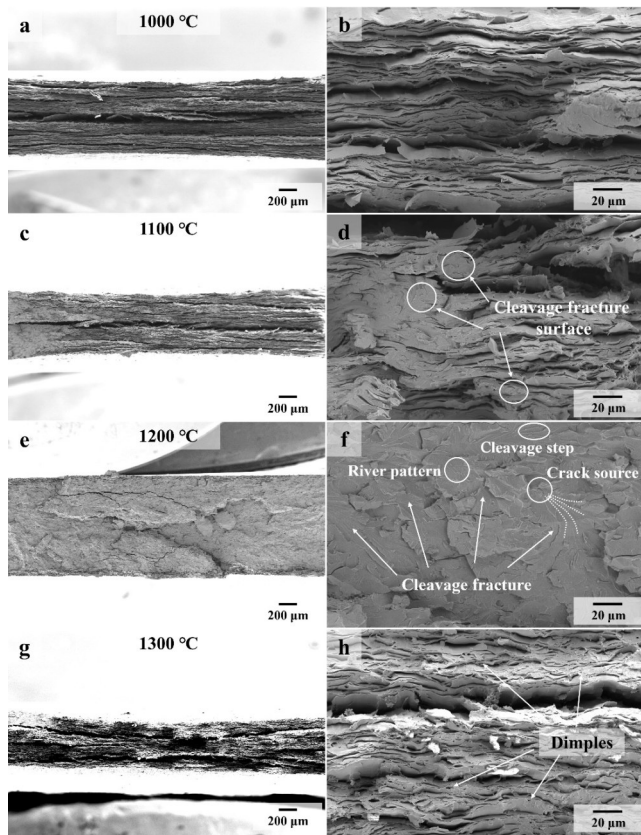


Fig.3 Microstructures of low-oxygen TZM alloys after solid-solution quenching at different temperatures: (a–b) 1000 °C; (c–d) 1100 °C; (e–f) 1200 °C; (g–h) 1300 °C

many deconstructive steps can also be seen (as shown in the oval circle in Fig.3f), and the starting point of fracture can be found by backward extrapolation of the direction of the river-like patterns. After solid-solution treatment at 1300 °C, the fracture of the sample is dominated by tear ribs and tough nests, showing obvious plastic deformation characteristics. By analyzing the fracture microstructure of low-oxygen TZM alloy after solid-solution quenching at different temperatures,

it can be concluded that with the increase in solid-solution temperature, the fracture mechanism of low-oxygen TZM alloy is gradually transformed from laminar tearing to perforated crystalline deconvolutional fracture, and the characteristic of plastic fracture is more and more obvious.

3.2 Three-point bending properties

It is extremely common for materials to be subjected to bending loads in practical applications, and the bending performance of materials can usually be tested through three-point or four-point bending tests on simply supported beams. Through the tensile experiment, it is concluded that the sample after solid-solution at 1200 °C has the optimal comprehensive performance. Therefore, the three-point bending test is conducted to measure the bending strength and modulus of low-oxygen TZM alloy plate after solid-solution quenching at 1200 °C. Since the flexural strength and flexural modulus of the material cannot be directly derived from the testing process, the following two formulas need to be used to calculate. The flexural strength formula is as follows:

$$\sigma_b = \frac{3Fl}{2bh^2} \tag{1}$$

where σ_b is bending strength; F is the load; l is the span; b and h mean the width and thickness of the sample, respectively. And the flexural modulus formula is as follows:

$$E_b = \frac{p^3 \Delta F}{4bh^3 \Delta f} \tag{2}$$

where E_b is bending modulus; ΔF is the load increment corresponding to the straight segment on the load-displacement curve; p is the support span, which is the distance between two support points, measured in meters (m); Δf is corresponding to the deflection at the midpoint of the span of Δp .

Fig. 4a shows the load-displacement curve obtained from room temperature three-point bending experiments of low-oxygen TZM alloys after solution-quenching at 1200 °C. The load-displacement curve of three-point bending can usually be divided into three stages, which include the elastic deformation stage, the yielding stage and the failure stage.

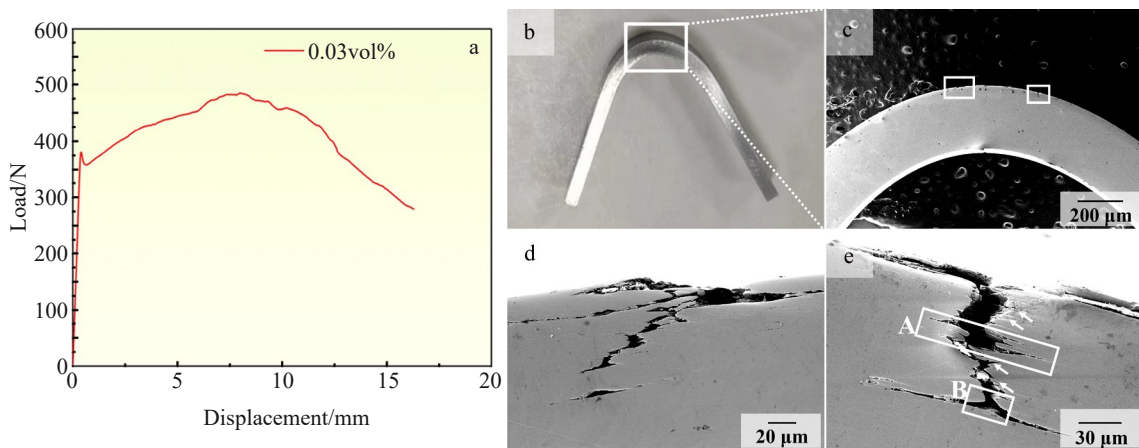


Fig.4 Load-displacement curve (a) and microstructures (b–e) obtained from room temperature three-point bending experiment of low-oxygen TZM alloy after solid-solution quenching at 1200 °C

During the loading process, the load increased rapidly with the increase in the displacement of the loading point. After the end of the elastic phase and a period of yielding process, the load reached the maximum value when the displacement reached 8.1 mm, and then the load decreased with the increase in displacement at the loading point until the sample fell without fracture. The flexural strength of the low-oxygen TZM alloy is calculated to be 1699.5 MPa, and the modulus of elasticity is 392.9 GPa.

The microstructure and morphology of low-oxygen TZM alloy after three-point bending at room temperature and solid solution quenching at 1200 °C are shown in Fig.4b–4e. The sample does not fracture during the loading process until the sample is dropped, and there is no crack visible to the naked eye on the surface, as shown in Fig.4b. The microstructure after three-point bending at room temperature was observed by SEM and the crack distribution was analyzed, as shown in Fig.4b–4d. In this experiment, the upper surface in contact with the three-point bending indenter is set as the upper surface, and the opposite surface is the lower surface. Due to the bending characteristics, the upper and lower surfaces of the sample are subjected to compressive and tensile stresses, and the failure is usually caused by the tensile stresses, resulting in surface cracking. Cracks propagate through continuous deformation, ultimately leading to failure.

Fig.4b shows the morphology of the sample at low magnification, from which the presence of cracks is hardly observed. Continuing the magnification, observation along the upper and lower edges reveals several fine cracks on the side subjected to tensile stress, as shown in Fig.4d–4e, corresponding to the locations of the two white boxes in Fig.4c. After the crack initiates on the surface, the expansion path moves forward in a zigzag shape and exhibits obvious branching phenomenon. And the crack exhibits obvious tearing phenomenon. The process of crack propagation can be clearly observed from Fig.4e, where A represents a brief passivation of the crack tip during the crack propagation process, but with deformation, the crack propagation starts again, the propagation direction changes, and small branches are generated. This process repeats in continuous deformation, producing multiple fine branches, as shown by the white arrow in Fig.4e. When the main crack expands to B, the passivation phenomenon occurs again, and then a new fine crack is generated before the passivated crack, which has a large angle with the original expansion direction. It indicates that there is a specific microstructure formation in the low-oxygen TZM alloy, which improves the strength of the grain boundaries and consumes more energy during crack propagation, thus passivating or changing the extension direction.

3.3 Changes in microstructure and grain boundaries

After solid-solution quenching, the residual oxide layer on the surface of the sample is polished, and then mechanical polishing and corrosion treatment are carried out to observe the changes in the microstructure of low-oxygen TZM alloy after solid-solution at different temperatures, as shown in Fig. 5. The microstructures of low oxygen TZM alloy after

solution quenching at 1000, 1100, 1200, and 1300 °C are consistent with those before solidification treatment. The grains are elongated along the rolling direction, and no obvious recrystallization zone is found. The secondary phase in the alloy is almost invisible to the naked eye, except for some agglomerated large-sized secondary-phase particles.

The IPFs of low-oxygen TZM alloy plates after solid-solution quenching at 1000, 1100, 1200, and 1300 °C are shown in Fig.6. It can be seen that in the samples after solid-solution treatment at different temperatures, the majority of grains remains elongated along the rolling direction, and there are no large recrystallized areas. But for the samples after solid-solution treatment at 1300 °C, small recrystallized grains can be clearly observed in various regions. The average grain sizes of low-oxygen TZM alloy sheets after solution quenching at different temperatures are shown in Table 3. With the increase in solid-solution temperature, the average grain size also gradually increases. The higher the temperature, the faster the grain growth rate.

Deformed metal undergoes static recovery or recrystallization after heating, and dynamic recovery or recrystallization occurs during direct thermal processing. The reply is that dislocations within the grains are deformed into polygons and further transformed into equiaxed sub-grains. During the

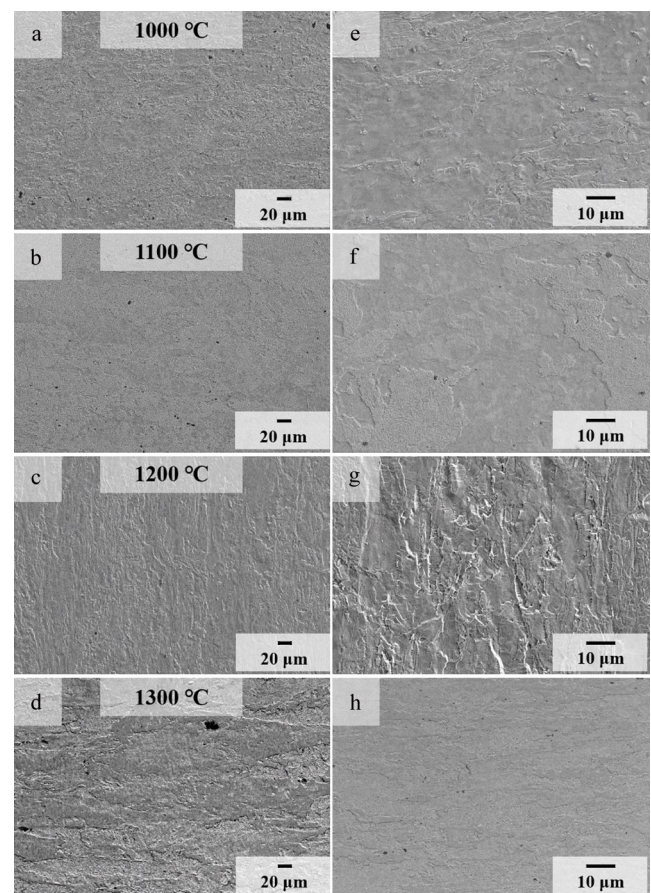


Fig.5 Microstructures of low-oxygen TZM alloy sheet after solid-solution quenching at different temperatures: (a, e) 1000 °C; (b, f) 1100 °C; (c, g) 1200 °C; (d, h) 1300 °C

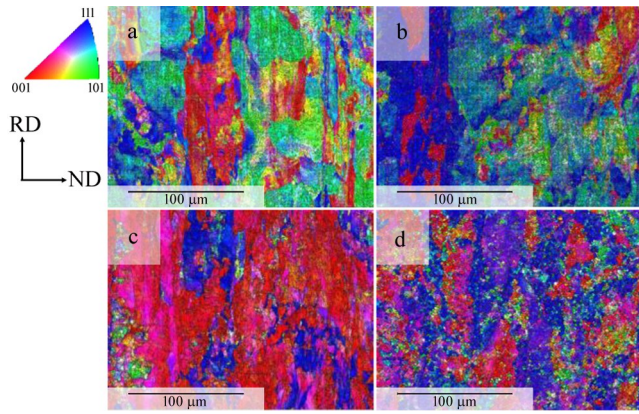


Fig.6 IPFs of low-oxygen TZM alloy sheet after solid-solution quenching at different temperatures: (a) 1000 °C; (b) 1100 °C; (c) 1200 °C; (d) 1300 °C

Table 3 Average grain sizes of low-oxygen TZM alloy sheets after solution quenching at different temperatures

Solid-solution temperature/°C	Average grain size/μm
1000	0.88±0.042
1100	0.99±0.033
1200	2.15±0.038
1300	2.30±0.055

polygonal process, sub-grain boundaries gradually appear within the originally deformed internal grains, and the orientation difference between adjacent sub-grain boundaries is generally between 2°–15°. The driving force for recrystallization is the deformation stored energy that is not released after recovery. After recrystallization, the orientation difference between adjacent grains further increases, becoming large angle grain boundaries (>15°). The analysis of the large and small angle grain boundaries shows that the small angle grain boundaries in the alloy are gradually transformed to large angle grain boundaries with increasing the solid-solution temperature, as shown in Fig. 7. Combined with Fig. 8, which shows the distribution of recrystallized grains (blue), substructural grains (yellow) and deformed grains (red) in low-oxygen TZM alloy plates after solidification-quenching at different temperatures, the degree of recrystallization increases with the increase in solidification temperature. And when the solidification temperature reaches 1300 °C, the percentage of recrystallized grains can reach more than 10%.

Fig.9 shows the kernel average misorientation (KAM) maps of low-oxygen TZM alloy plates after solution quenching at different temperatures. As shown in Fig.9a–9d, after solution quenching at different temperatures, dislocations are densely distributed in the low-oxygen TZM alloy, showing that the dislocations have a tendency to increase and then decrease with the increase in temperature. This is mainly due to the higher solution temperature and longer holding temperature of 12 h, which continue the recrystallization process and

consume dislocations. This phenomenon becomes more prominent with the increase in temperature, and the dislocation density is relatively the lowest in the microstructure after solution quenching at 1300 °C.

3.4 Evolution of secondary phase of low-oxygen TZM alloys

After solid-solution quenching of low-oxygen TZM alloy, SEM observation shows that the number of visible secondary phases in the microstructure is very small. The difference in microstructure after treatments at different temperatures is minimal, but there are significant differences in alloy properties. Therefore, TEM and EDS analyses were conducted on low-oxygen TZM after solid-solution quenching at different temperatures. Fig. 10 shows the TEM and EDS analysis results of low-oxygen TZM alloy plate after solution quenching at 1000 °C.

From Fig. 10a, it can be seen that at low magnification, there is no obvious presence of small secondary phase particles observed in the TZM alloy. Whereas under high magnification, enrichment of nanoscale particles appear in a very small number of local areas (Fig. 10c). EDS element mappings (Fig. 10d) indicate that the enriched particle phase at this location is mainly titanium oxide particle, with much smaller nano-enriched titanium phases distributed around it. Combined with Fig. 10c, the distribution of titanium oxide is mainly along the grain boundaries due to the susceptibility of elemental O to segregation at the grain boundaries, while the other nanoscale Ti-rich phases are uniformly distributed around the titanium oxide.

Fig. 11 shows the TEM images and EDS element mappings of low-oxygen TZM alloy plate after solution quenching at 1100 °C. Similar to 1000 °C, small secondary phase particles cannot be seen at low magnification, but there are large secondary-phase particles at the edge grain boundaries (Fig. 8b). Through EDS analysis, they are composite oxides of titanium and zirconium. These large secondary-phase oxide particles will become the source of cracks in material plastic deformation, leading to the deterioration of material properties. After solid-solution quenching at 1100 °C, only a small number of nanoparticles appear, which is consistent with the EDS analysis of alloy at 1000 °C. This is the secondary phase of titanium oxide and the nanoscale Ti-rich phase.

As shown in Fig. 12, in the low-oxygen TZM alloy solution quenched at 1200 °C, although the magnification is low, a large number of nanoscale precipitates can already be seen which are diffused and distributed in the alloy, as indicated by the red arrow. Under larger magnification, it can be seen that a large number of nanoscale phases precipitate from the alloy and are more evenly distributed in the material (Fig. 12c). After EDS analysis, the main nanoparticles precipitated from alloy after solid-solution quenching at 1200 °C are rich in titanium phase, accompanied by a small amount of titanium oxide phase biased at the grain boundaries. This is mainly due to the high heating temperature and long holding time during the solid-solution process at 1200 °C, which can provide

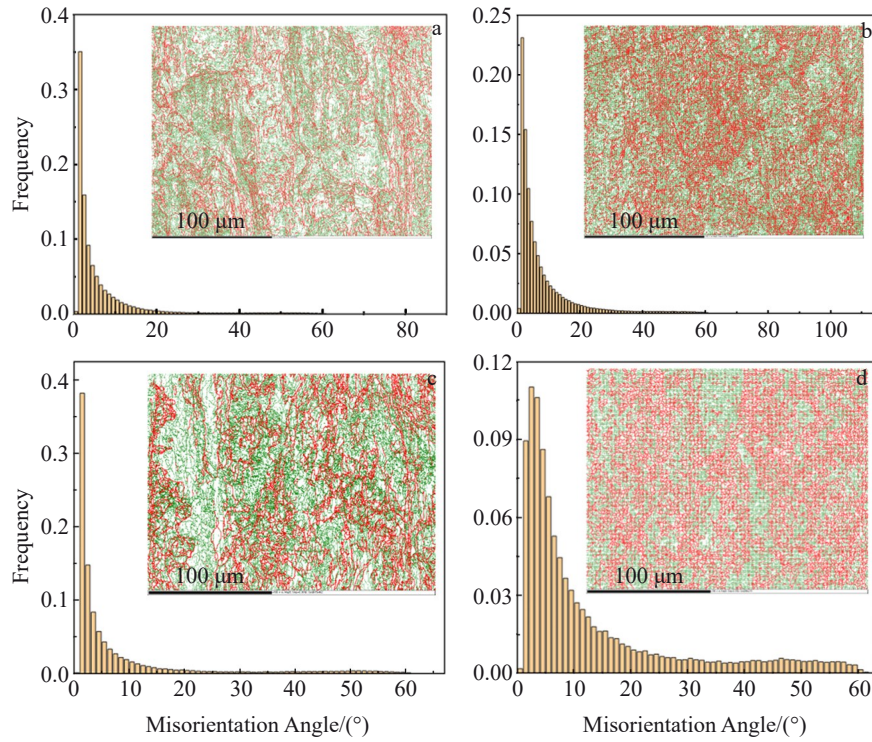


Fig.7 Grain boundary maps and misorientation angle distributions of low-oxygen TZM alloy sheet after solid-solution quenching at different temperatures: (a) 1000 °C; (b)1100 °C; (c)1200 °C; (d) 1300 °C

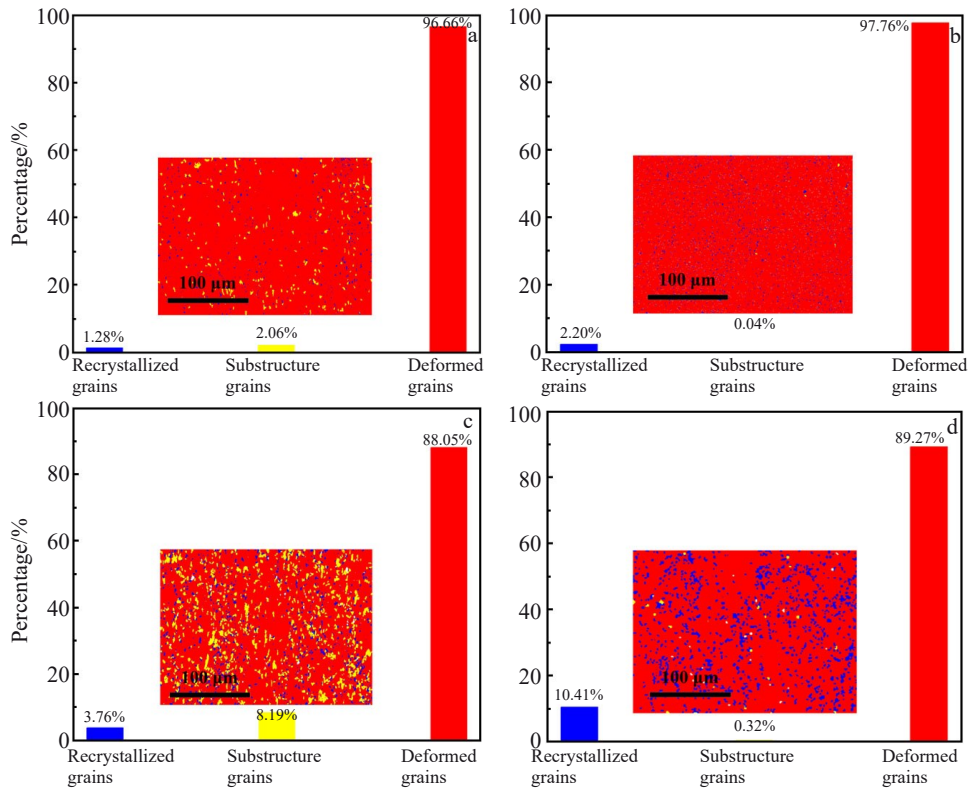


Fig.8 Grain distributions of low-oxygen TZM alloy sheet after solid-solution quenching at different temperatures: (a) 1000 °C; (b) 1100 °C; (c) 1200 °C; (d) 1300 °C

sufficient energy for the smooth precipitation of Ti atoms during quenching. The size statistics of the precipitated

nanophase in this sample indicate an average particle size of approximately 10 nm. In addition, nano-sized titanium oxide

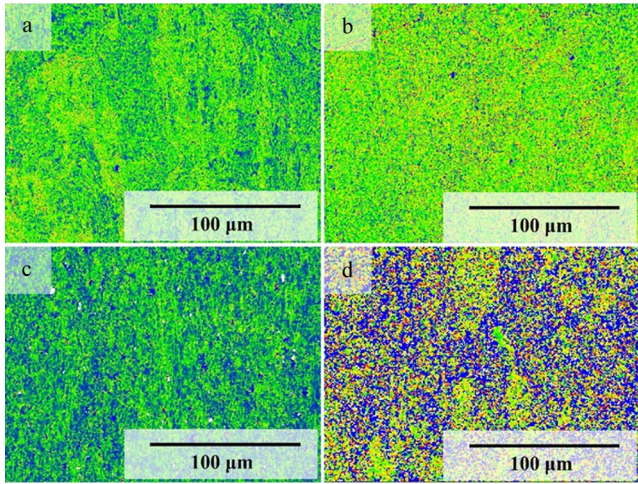


Fig.9 KAM maps of low-oxygen TZM alloy sheet after solid-solution quenching at different temperatures: (a) 1000 °C; (b) 1100 °C; (c) 1200 °C; (d) 1300 °C

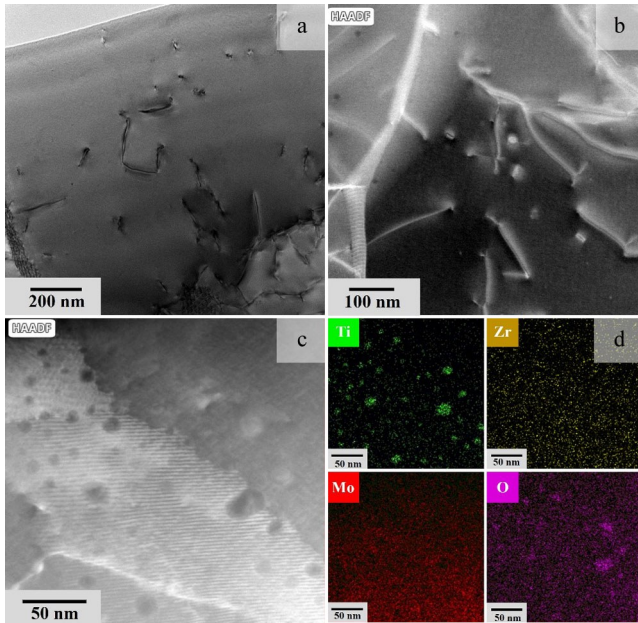


Fig.10 TEM images (a–c) and EDS element mappings (d) of low-oxygen TZM alloy plate after solid-solution quenching at 1000 °C

particles partially located at grain boundaries are found in the solid-solution of the sample quenched at 1200 °C. In this sample, it is also found that some nanoscale titanium oxide particles are located at grain boundaries.

Fig. 13 shows TEM images and EDS analysis of low-oxygen TZM alloy plate after solution quenching at 1300 °C. Similar to the solid-solution treatment at 1200 °C, a large number of nanoscale particles are distributed in the matrix, as indicated by the red arrows. When the magnification increases, a large number of nanoscale precipitates can be seen, some of which are more evenly distributed in the material (compared to Fig.13c), and some are in the form of

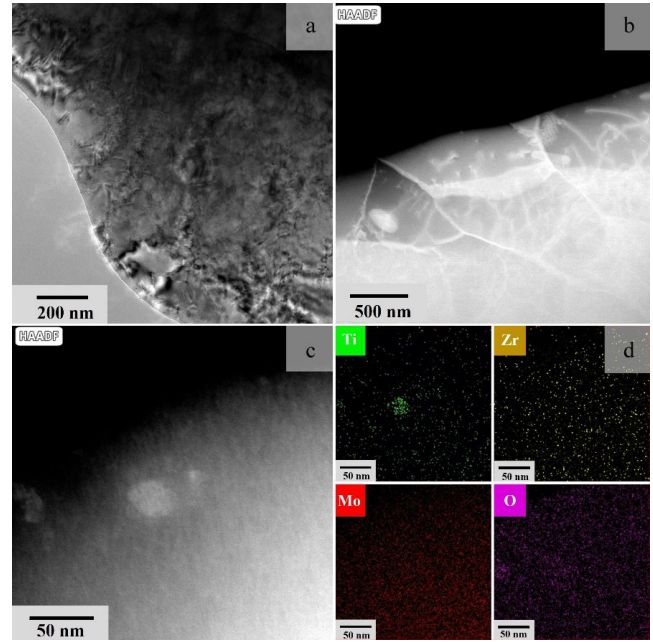


Fig.11 TEM images (a–c) and EDS element mappings (d) of low-oxygen TZM alloy plate after solid-solution quenching at 1100 °C

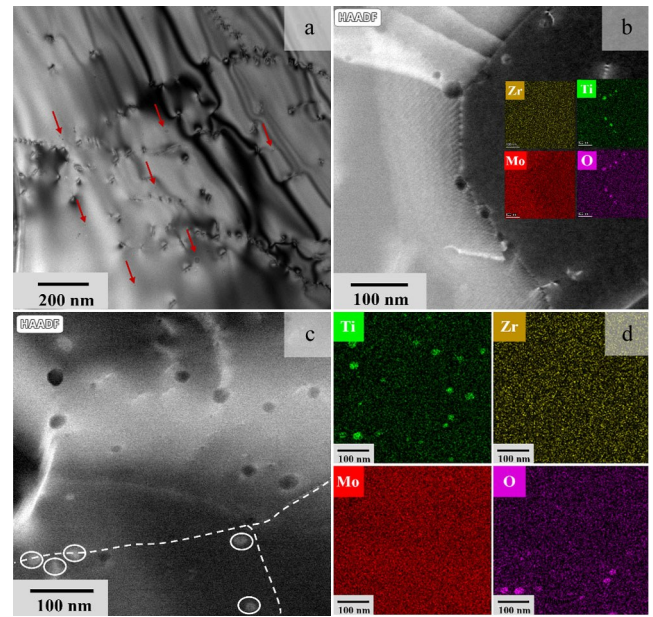


Fig.12 TEM images (a–c) and EDS element mappings (d) of low-oxygen TZM alloy plate after solid-solution quenching at 1200 °C

bands (Fig.13b). According to EDS analysis, the precipitated nanoparticles are all Ti-rich phases. The size statistics of the precipitated nanoparticles in the 1300 °C solidified sample show that the average particle size is about 21 nm, which is increased compared to the size of the precipitated phase in the 1200 °C solidified sample.

Of interest, a large number of aggregated nano-precipitated phases are found in the low-oxygen TZM alloy after solid-

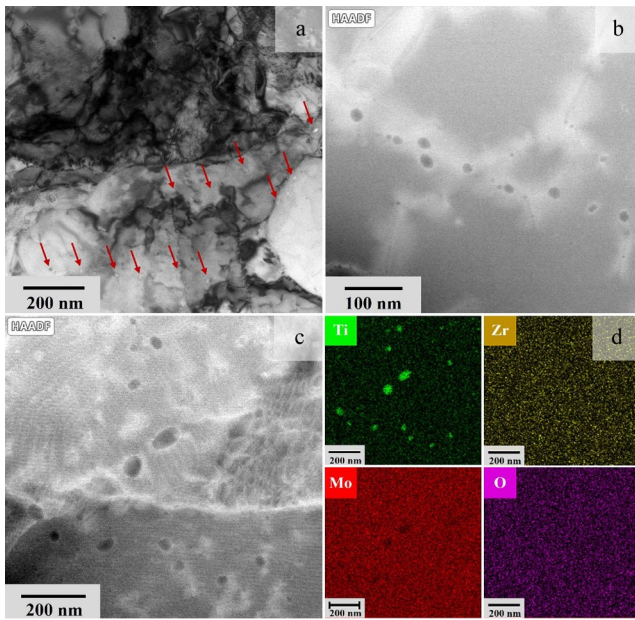


Fig.13 TEM images (a–c) and EDS element mappings (d) of low-oxygen TZM alloy plate after solid-solution quenching at 1300 °C

solution quenching at 1200 °C, accompanied by a striped precipitation path next to it. In order to determine the composition of the nanophase in this region, the band-shaped region is magnified and analyzed by EDS, and the results are shown in Fig. 14. The nanoparticles in the band-shaped region and the aggregation region (indicated by the blue arrow in Fig.14a) are nano-titanium oxide particles (TiO_2).

The nucleation of precipitates within the alloy matrix

requires overcoming the activation energy barrier, which is the primary task for effective nucleation. The solution treatment of low-oxygen TZM alloy at high temperature gives the dissolved atoms an intrinsic driving force to initiate nucleation. In addition, the driving force intensity of precipitation behavior is directly proportional to the supersaturation of the solute, i.e., it increases with the increase in supersaturation. For TZM alloys with an oxygen content of up to 0.03vol%, the element Zr captures a large number of oxygen atoms and forms zirconia, resulting in a significant increase in the number of Ti atoms available for precipitation reactions in the system. The rapid cooling of solid solution alloys using ice water as a quenching medium not only leads to a sudden decrease in alloy temperature, thereby improving the nucleation efficiency of precipitates, but also ensures that the Ti-rich phase maintains its typical body-centered cubic crystal structure. It is worth noting that precipitates typically have a unique chemical composition that is different from the entire Mo alloy matrix, and their generation is inevitably accompanied by local microstructure of the chemical composition. This microstructural phenomenon essentially depends on the operation of atomic diffusion mechanisms, and without the presence of atomic vacancies, it cannot be effectively carried out.

Before the rolling pretreatment of low-oxygen TZM alloy, this measure provides a rich source of vacancies for the precipitation of Ti atoms during the subsequent solid-solution quenching process. The phenomenon of increasing vacancy concentration with temperature further promotes the precipitation reaction. In summary, in the TZM alloy system with an oxygen content of 0.03vol%, due to the combined effect of thermodynamic stability and precipitation kinetics

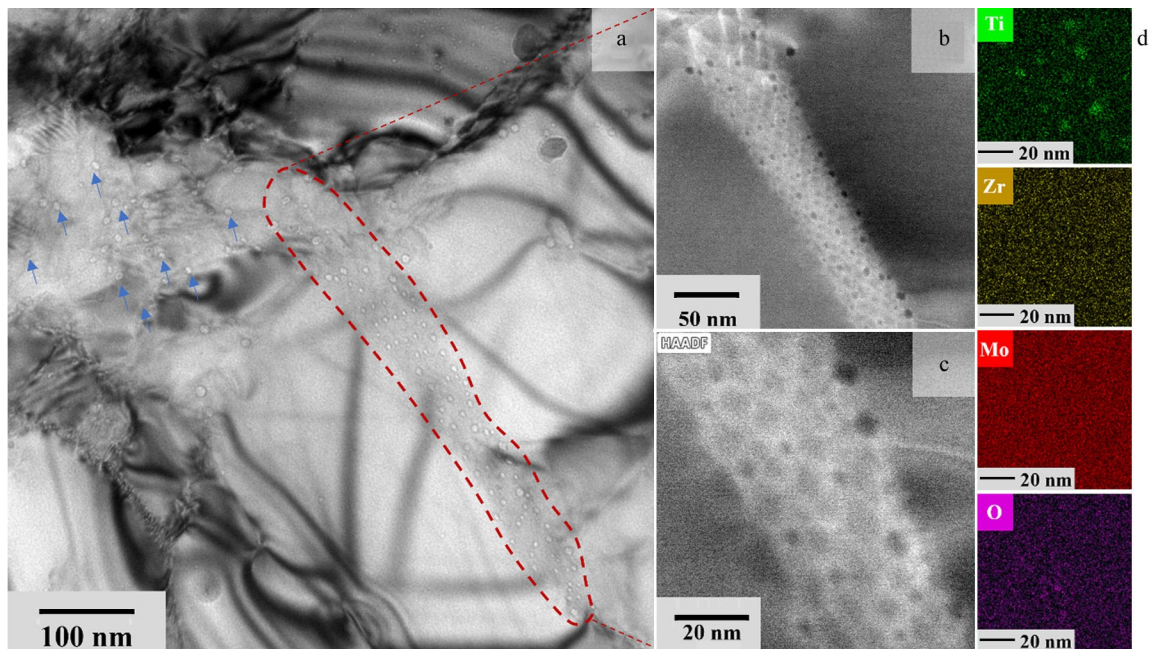


Fig.14 TEM images of nanoscale Ti-rich phases in low-oxygen TZM alloy sheet after solid-solution quenching at 1200 °C (a–c); EDS element mappings corresponding to Fig.14c (d)

rate, the sample exhibits the highest precipitation nucleation rate at higher solid-solution temperatures. As the temperature increases, Ti atoms diffuse faster and accumulate in vacancies, and some of these atoms undergo maturation and growth phenomena. Therefore, the size of the precipitated phase in the sample after solid-solution treatment at 1300 °C is larger than that at 1200 °C. These nanoscale precipitated Ti-rich phases play a good role in hindering dislocation slip during alloy deformation, without causing dislocation accumulation. On the one hand, the pinning and channeling of nanoscale Ti-rich phase relative to dislocations can harden TZM alloys to a high level. On the other hand, the nanoscale Ti-rich phase avoids dislocation accumulation and stress concentration relative to the channels of dislocations, thereby ensuring the uniform distribution of dislocations throughout the material. The significant improvement in plasticity of TZM alloy samples with an oxygen content of 0.03vol% is attributed to the elimination of the secondary phase of coarse oxide, in-situ precipitation of fine nanoscale Ti-rich phase after solution quenching, and the increase in grain boundary strength caused by the decrease in oxygen content.

4 Conclusions

1) The tensile strength of low-oxygen TZM alloy gradually decreases with the increase in solution temperature, and the elongation firstly increases and then decreases. When the solution temperature is 1000 °C, the tensile performance of low-oxygen TZM alloy has the highest tensile strength of 902 MPa. When the solid solution temperature is 1200 °C, the optimal elongation of low oxygen TZM alloy is 28.1%.

2) The low-oxygen TZM alloy after solution quenching at 1200 °C has good three-point bending properties, with bending strength and bending modulus of 1699.5 MPa and 392.9 GPa, respectively.

3) With the increase in solid-solution temperature, there is no significant change in the microstructure of low-oxygen TZM alloy, while the average grain size gradually increases and the dislocation density gradually decreases.

4) After solution quenching, nanoscale Ti-rich phases and nanoscale titanium oxide particles appear in the low-oxygen TZM alloy. The number of nanoscale Ti-rich phases in the alloy gradually increases with the increase in solution temperature, and their size also slightly increases.

References

- Li Xingyu, Zhang Lin, Wang Guanghua et al. *International Journal of Refractory Metals and Hard Materials*[J], 2020, 92: 105294
- Mantri S A, Choudhuri D, Alam T et al. *Scripta Materialia*[J], 2017, 130: 69
- Primig S L, Leitner H, Clemens H et al. *International Journal of Refractory Metals and Hard Materials*[J], 2010, 28: 703
- Lunk H J, Hartl H. *The Textbook Journal of Chemistry*[J], 2017, 3: 13
- Feng Pengfa, Yang Qinli, Dang Xiaoming et al. *Chinese Journal of Rare Metals*[J], 2017, 41(1): 57 (in Chinese)
- Schneibel J H, Brady M P, Kruzic J J et al. *International Journal of Materials Research*[J], 2022, 96(6): 632
- Cockeram B V. *Metallurgical and Materials Transactions A*[J], 2009, 40(12): 2843
- Liu G, Zhang G J, Jiang F et al. *Nature Materials*[J], 2013, 12(4): 344
- Wang M, Yang S P, Liu H J et al. *Rare Metal Materials and Engineering*[J], 2021, 50(9): 3158
- Endoh K, Tahara M, Inamura T et al. *Journal of Alloys and Compounds*[J], 2017, 695:76
- Lang D, Pohl C, Holec D et al. *Journal of Alloys and Compounds*[J], 2016, 654: 445
- Yavas B, Goller G. *International Journal of Refractory Metals and Hard Materials*[J], 2016, 58: 182
- Yao Liying, Gao Yimin, Li Yefei et al. *Journal of Alloys and Compounds*[J], 2022, 921: 166155
- Xu Liujie, Li Na, Song Wanli et al. *Journal of Alloys and Compounds*[J], 2022, 897: 163110
- Wang Miao, Yang Shuangping, Dong Jie et al. *Materials*[J], 2022, 15(5): 1958
- Hu Boliang, Wang Kuaishe, Hu Ping et al. *Materials Science and Engineering A*[J], 2019, 759: 167
- Yang Pingjiong, Li Qingjie, Tsuru T et al. *Acta Materialia*[J], 2019, 168: 331
- Kaserer L, Braun J, Stajkovic J et al. *International Journal of Refractory Metals and Hard Materials*[J], 2020, 93: 105369
- Hu Boliang, Wang Kuaishe, Hu Ping et al. *International Journal of Refractory Metals and Hard Materials*[J], 2020, 92: 105336
- Xing Hairui, Hu Ping, He Caojun et al. *Journal of Materials Science & Technology*[J], 2023, 160: 161
- Hu Ping, Li Hui, Zuo Yegai et al. *Materials Characterization*[J], 2021, 173: 110933
- Dai Baozhu, Wei Shizhong, Peng Guanghui et al. *Hot Working Technology*[J], 2009, 38(14): 51 (in Chinese)
- Wang Kuaishe, Hu Ping, Li Shilei et al. *Materials Characterization*[J], 2022, 186: 111800
- Liu G, Zhang G J, Jiang F et al. *Nature Materials*[J], 2013, 12(4): 344
- Liu G F, Chen T J, Wang Z J. *Materials Science and Engineering A*[J], 2021, 817: 141413
- Lei Zhifei, Liu Xiongjun, Wu Yuan et al. *Nature*[J], 2018, 563(7732): 546

固溶热处理对低氧 TZM 合金组织和力学性能的影响

邢海瑞¹, 史茜霜^{1,4}, 胡卜亮¹, 李世磊^{1,3}, 李延超³, 王 华², 王 强⁴, 徐流杰⁵,
冯 锐⁴, 张 文³, 胡 平¹, 王快社¹

(1. 西安建筑科技大学 冶金工程学院 功能材料加工国家与地方联合工程研究中心, 陕西 西安 710055)

(2. 西安建筑科技大学 环境与市政工程学院, 陕西 西安 710055)

(3. 西北有色金属研究院 难熔金属材料研究所, 陕西 西安 710016)

(4. 西部鑫兴稀贵金属有限公司, 陕西 商洛 726100)

(5. 河南科技大学 金属材料磨损控制与成型国家联合工程研究中心, 河南 洛阳 471003)

摘 要: 研究了低氧 (氧含量为 0.03vol%) TZM 合金, 在不同温度下对其进行固溶热处理, 然后淬火。结果表明, 合金的抗拉伸强度随着固溶温度的升高而逐渐降低, 伸长率先增加后降低。随着固溶温度的升高, 低氧 TZM 合金中析出的纳米级富钛相的含量逐渐增加。在 1200 和 1300 °C 下凝固的样品中出现了特殊的条形富钛区域。纳米级富钛相确保了位错在整个 TZM 合金中的均匀分布, 同时显著提高了低氧 TZM 合金样品的塑性。

关键词: TZM 合金; 固溶体; 淬火; 微观结构演变; 力学性能

作者简介: 邢海瑞, 女, 1996 年生, 博士, 西安建筑科技大学冶金工程学院功能材料加工国家与地方联合工程研究中心, 陕西 西安 710055, E-mail: hairui@xauat.edu.cn